Biochimica et Biophysica Acta 1818 (2012) 520–529

Contents lists available at SciVerse ScienceDirect

Biochimica et Biophysica Acta

journal homepage: www.elsevier.com/locate/bbamem

# Saturation with cholesterol increases vertical order and smoothes the surface of the phosphatidylcholine bilayer: A molecular simulation study

Elżbieta Plesnar [a], Witold K. Subczynski [b], Marta Pasenkiewicz-Gierula [a,*]

[a] Department of Computational Biophysics and Bioinformatics, Faculty of Biochemistry, Biophysics and Biotechnology, Jagiellonian University, Krakow, Poland
[b] Department of Biophysics, Medical College of Wisconsin, Milwaukee, Wisconsin, USA

ARTICLE INFO

*Article history:*
Received 6 June 2011
Received in revised form 22 September 2011
Accepted 24 October 2011
Available online 29 October 2011

*Keywords:*
Fiber-cell membrane
Eye lens
Lens transparency
Chain order
Isomerization

ABSTRACT

Molecular dynamics (MD) simulations of a mono-*cis*-unsaturated 1-palmitoyl-2-oleoyl-phosphatidylcholine (POPC) bilayer and a POPC bilayer containing 50 mol% cholesterol (POPC–Chol50) were carried out for 200 ns to compare the spatial organizations of the pure POPC bilayer and the POPC bilayer saturated with Chol. The results presented here indicate that saturation with Chol significantly narrows the distribution of vertical positions of the center-of-mass of POPC molecules and POPC atoms in the bilayer. In the POPC–Chol50 bilayer, the same moieties of the lipid molecules are better aligned at a given bilayer depth, forming the following clearly separated membrane regions: the polar headgroup, the rigid core consisting of steroid rings and upper fragments of the acyl chains, and the fluid hydrocarbon core consisting of Chol chains and the lower fragments of POPC chains. The membrane surface of the POPC–Chol50 bilayer is smooth. The results have biological significance because the POPC–Chol50 bilayer models the bulk phospholipid portion of the fiber-cell membrane in the eye lens. It is hypothesized that in the eye lens cholesterol-induced smoothing of the membrane surface decreases light-scattering and helps to maintain lens transparency.



## 1. Introduction

Fiber-cell membranes of the human eye lens are overloaded with cholesterol (Chol) [1,2]. Generally, when Chol exceeds the phospholipid-Chol miscibility threshold in the membrane, immiscible cholesterol bilayer domains (CBDs) within phospholipid-cholesterol domain saturated with Chol (PCD), start to form [3–5]. It is hypothesized that a high amount of Chol and the presence of CBDs help to maintain lens transparency [3,6,7] and, therefore, possibly protect against cataract formation [3,8]. However, their particular role in fiber-cell membranes of the human eye lens has not been determined.

Better understanding of the physiological role of membrane saturation with Chol requires improved molecular-level knowledge of the interactions between Chol and membrane lipids. We have investigated experimentally, using EPR spin-labeling methods, the properties of the phospholipid-cholesterol domain saturated with cholesterol, PCD, in lens lipid membranes from different animals (cow and pig [9–11]), from animals at different ages (six-month- and two-year-old cows [10–12]), and from different eye regions (the cortex and nucleus of two-year-old cows [12]). The phospholipid composition of the fiber-cell membrane is significantly different for different species [13–15], ages [15], and regions of the lens [16]. The phospholipids differ both in the chemical structure of their headgroups and the degree of saturation of their acyl chains. Nevertheless, depth dependences (profiles across the bilayer) of quantities characterizing the bulk membrane, including order parameter, hydrophobicity, and oxygen transport parameter (oxygen diffusion–concentration product), are nearly identical in all of the investigated membranes. Therefore, we concluded that a saturating content of Chol in the fiber-cell membrane keeps the bulk physical properties of the PCD the same independently of the phospholipid composition. The profiles mentioned above are very similar when the CBD is not yet formed in the membrane and when it is already formed (*i.e.*, in the PCD surrounding the CBD [9,12]), the latter of which is the case of membranes in aged eyes. This allowed us to conclude further that the CBD plays some role specific to the fiber-cell plasma membrane. The CBD provides a buffering capacity for Chol concentration in the surrounding phospholipid bilayer, keeping it at a constant saturating level to ensure certain physical properties of the membrane. These results are especially significant for human lenses. Among mammalian lenses, human lenses have the longest lifespan and changes in their phospholipid composition due to age are the most pronounced [17].

*Abbreviations:* CBD, cholesterol bilayer domain; PCD, phospholipid–cholesterol domain; PC, phosphatidylcholine; POPC, 1-palmitoyl-2-oleoyl-phosphatidylcholine; Chol, cholesterol; MD, molecular dynamics; CM, center-of-mass; RP, roughness parameter

* Corresponding author at: Department of Computational Biophysics and Bioinformatics, Faculty of Biochemistry, Biophysics and Biotechnology, Jagiellonian University, ul. Gronostajowa 7, 30-387 Krakow, Poland. Tel.: +48 12 664 6518; fax: +48 12 664 6902.
*E-mail addresses:* elzbieta.pieniazek@uj.edu.pl (E. Plesnar), subczyn@mcw.edu (W.K. Subczynski), marta.pasenkiewicz-gierula@uj.edu.pl (M. Pasenkiewicz-Gierula).

0005-2736/$ – see front matter © 2011 Elsevier B.V. All rights reserved.
doi:10.1016/j.bbamem.2011.10.023

To achieve a better understanding of the properties of the lens lipid membrane, we also carried out EPR spin-labeling studies of 1-palmitoyl-2-oleoyl-phosphatidylcholine (POPC) bilayers in the cholesterol-dependent liquid-ordered phase. A POPC–Chol bilayer (like other phosphatidylcholine [PC] bilayers) is in the liquid-ordered phase when the Chol content is between 30 and 50 mol%. Below this range (but above ~7 mol%), the liquid-disordered and liquid-ordered phases coexist, and above this range, a pure Chol bilayer domain (CBD) starts to form in the bilayer. Thus, 50 mol% is an approximate saturating Chol content for the POPC bilayer. When the Chol content reaches saturation, the most drastic changes that occur in the bilayer are observed in the profiles of hydrophobicity and the oxygen transport parameter [18,19]. In liquid-ordered PC bilayers of the lowest Chol content of ~30 mol%, as well as in bilayers without Chol, these profiles are bell-shaped [20,21]. At Chol saturation, the shape of these profiles becomes rectangular and is practically the same as for lens lipid membranes [22,23]. The discontinuities in these profiles (an abrupt increase) occur near the vertical positions of the ninth (C9) and tenth (C10) carbon atoms in the acyl chains (*i.e.*, approximately at the depth at which the rigid tetracyclic Chol structure is immersed in the bilayer). Hydrophobicity profiles were obtained experimentally for frozen membranes where lipid motions were halted [10]. Alternatively, profiles of the oxygen transport parameter were obtained at physiological temperatures for liquid-crystalline membranes [10,11]. In the bilayer saturated with Chol, the oxygen transport parameter from the membrane surface to the approximate depth of C9 was as low as in a gel-phase membrane, and at locations deeper than C9, it was as high as in the fluid-phase membrane. Thus, the abrupt increase in the parameter value in both bilayer leaflets occurs within the distance of one carbon–carbon bond (*i.e.*, 1.3–1.5 Å). This is difficult to explain unless one assumes that at a saturating Chol content the vertical fluctuations of lipid atoms are smaller than in membranes below a saturating Chol content. As a result, the vertical alignment of all corresponding lipid groups is high, and all Chol rings are immersed to the same membrane depth, which is close to the position of C9 in PC acyl chains. To determine the shapes of the profiles, very small probes (*i.e.*, molecular oxygen and the nitroxide moiety) are used [18]. Thus, the best way to confirm the effect of Chol on vertical alignment in the membrane is to use molecular dynamics (MD) simulation with atomic resolution. Atomistic MD simulations have proven to be extremely useful in membrane research (see [24] and references therein). They provide direct information about atomic level mechanisms not accessible by any of the current experimental techniques. Additionally, MD simulated systems are not perturbed by any probe as is often the case in experimental studies.

In the present research, we used an atomistic MD simulation method to characterize depth-dependent dynamic structures of a liquid-ordered POPC bilayer containing 50 mol% Chol and a liquid-disordered POPC bilayer without Chol. Comparison of these bilayers indicates that saturation with Chol significantly narrows the distribution of vertical positions of each lipid atom at all bilayer depths. As a result, the phospholipid bilayer surface becomes smoother, which is in accord with our hypothesis based on the experimental results discussed above.

We believe that these data contribute to a better understanding of the role of Chol in maintaining eye-lens transparency. We hypothesize that cholesterol-induced smoothing of the membrane surface should decrease light-scattering and help to maintain lens transparency.

## 2. Methods

### 2.1. System description and parameters

Atomic-scale MD simulations of two membrane systems (each composed of 200 lipid molecules) were performed. One system comprised only POPC (Fig. 1a) (POPC bilayer), and the other POPC and Chol (Fig. 1b) molecules (1:1 ratio) (POPC–Chol50 bilayer).

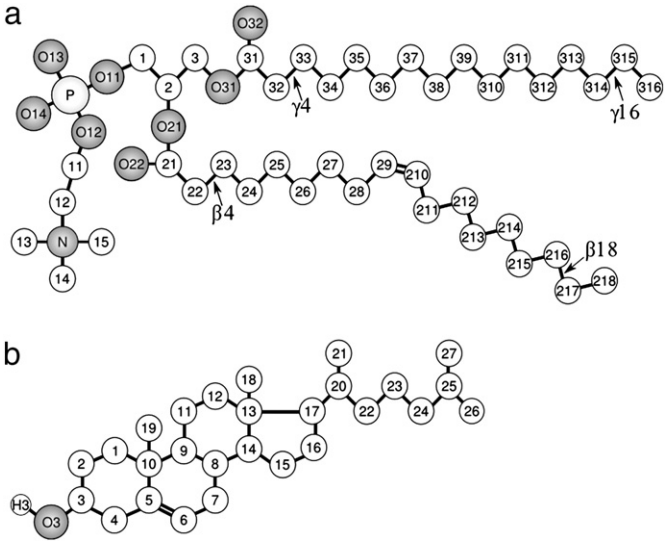


**Fig. 1.** Molecular structures with numbering of atoms of POPC (a) (according to Sundaralingam's nomenclature [61]) ("2" signifies oleoyl and "3" the palmitoyl chain) and Chol (b) molecules (the hydrogen atoms as well as the chemical symbol for carbon atoms, C, are omitted). Torsion angles at the beginning and end of each acyl chain are indicated.

Each of the bilayers was hydrated with 6000 water molecules (30 $H_2O$/lipid). Bilayers were constructed in two steps. First, 100 vertically oriented (along the *z*-axis) molecules (either POPC or POPC and Chol) were placed regularly in alternating POPC and Chol stripes in the *x*, *y* plane to form one layer (Fig. S1, Supplementary Material). Then, the second layer was obtained from the first by a 180° rotation and shifting to reduce the free volume between the layers. Each bilayer was simulated for over 200 ns using the GROMACSv4.0 software package [25]. The initial structure of Chol was the crystal structure of cholesterol molecule A, as determined by Shieh et al. [26], and that of POPC was taken from our previous bilayer system [27]. Hydrogen atoms were added to both structures.

For POPC and Chol molecules, all-atom optimized potentials for liquid simulations (OPLS-AA) [28] were used. For water, the transferable intermolecular potential three-point model (TIP3P) was used [29]. The linear constraint solver (LINCS) algorithm [30] was used to preserve the length of any covalent bond with a hydrogen atom, and the time step was set to 2 fs. The van der Waals interactions were cut off at 1.0 nm. Long-range electrostatic interactions were evaluated using the particle-mesh Ewald summation method with a β-spline interpolation order of 5 and direct sum tolerance of $10^{-5}$ [31]. For the real space, a cut-off of 1.0 nm, three-dimensional periodic boundary conditions, and the usual minimum image convention were used [31].

MD simulations were carried out in the *NPT* ensemble (the number of particles, pressure, and temperature were constant) at a pressure of 1 atm and temperature of 310 K, which is above the main-phase transition temperature for a pure POPC bilayer of −5 °C [32]. The temperatures of the solute and solvent were controlled independently by the Nose–Hoover method [33], with the relaxation time set at 0.6 ps. Pressure was controlled anisotropically by the Parrinello–Rahman method [34], with the relaxation time set at 1.0 ps. The list of nonbonded pairs was updated every five steps.

## 3. Results

### 3.1. Characterization of the membranes

#### 3.1.1. Equilibration

In the molecular modeling study of a lipid bilayer, the convergence of the surface area of the bilayer is an adequate first indicator of the

bilayer thermal equilibration. Fig. 2 shows time profiles of the POPC–Chol50 bilayer potential energy (Fig. 2a) and the surface area, together with the profile of the surface area of the POPC bilayer (Fig. 2b), from the onset of simulation until 200 ns. At a steady state, these parameters should remain constant. As Fig. 2a and b show, for the POPC–Chol50 bilayer both the potential energy and the area of the simulation box stabilized within 80 ns of MD simulation. The surface area of the POPC bilayer stabilized within a shorter time. For analysis, the last 100-ns fragment of the trajectory generated in 200-ns of MD simulation of each bilayer was used. Fig. S1 (Supplementary Material) indicates that the initial regular arrangement of the molecules in the POPC–Chol50 bilayer is lost after 100 ns due to translational diffusion (Fig. S2, Supplementary Material). Within 200 ns of MD simulation, displacement of the molecules is limited but, nevertheless, large enough to destroy the initial bilayer structure. Snapshots of the POPC and POPC–Chol50 bilayers at the end of the respective 200-ns trajectories are shown in Fig. 3.

The values reported below are time averages over the 100-ns trajectory generated in the production run (100–200 ns) and the ensemble of molecules or their fragments. Errors in the derived average values are standard deviation estimates.

### 3.1.2. Membrane thickness and cross-sectional area per lipid

Bilayer thickness is evaluated as the distance between the average positions of phosphorus (P) atoms in the two leaflets of a bilayer (P–P distance) and can be used as a comparative quantity. The average P–P distance in the POPC bilayer is $39.2 \pm 3.3$ Å, and in the POPC–Chol50 bilayer, it is $45.7 \pm 2.6$ Å (Table 1). Thus Chol, as expected, increases the membrane thickness. Concomitant with the increase, Chol causes a decrease in the average cross-sectional area/POPC ($A_{POPC}$) from $65.3 \pm 1.1$ Å$^2$ in the POPC bilayer to $48.9 \pm 2.7$ Å$^2$ in the POPC–Chol50 bilayer (Table 1). The average surface area per POPC in the POPC–Chol50 bilayer was obtained by subtracting the mean cross-sectional area of 50 Chol molecules ($50 \times A_{Chol}$) from the total surface area of the membrane and then dividing it by 50 (*i.e.*, the number of POPC molecules present in each leaflet) [35,36]. The mean surface area of a Chol molecule ($A_{Chol}$) in the Chol crystal [26] is ~37 Å$^2$, and in a Chol monolayer is ~39 Å$^2$ [37]. Our MD simulations of a pure Chol bilayer at 310 K give an average cross-sectional area per Chol of $37.9 \pm 0.1$ Å$^2$ (results to be published elsewhere) and this value was used to estimate the $A_{POPC}$ in the POPC–Chol50 bilayer. Values of the average cross-sectional area per POPC and Chol indicate a significant Chol condensing effect [37] in the POPC–Chol50 bilayer, but the main conclusions of this paper do not depend on exact values for $A_{Chol}$ and $A_{POPC}$ (see Section 4, Discussion).

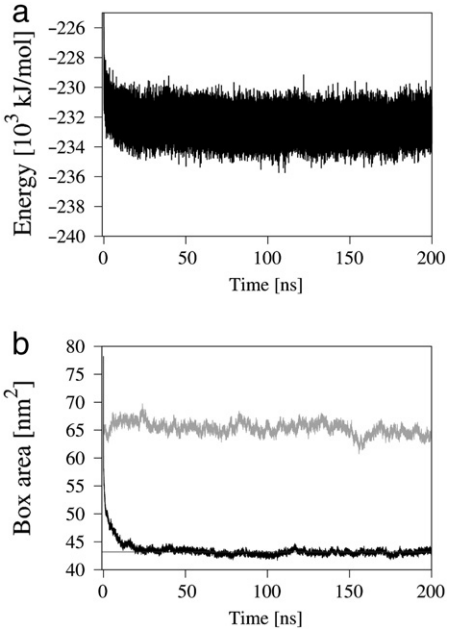


**Fig. 2.** Time profiles of the POPC–Chol50 bilayer potential energy (a), and the simulation box surface area (black line) together with that for the POPC bilayer (gray line) (b), from the onset of MD simulations. The thin line in panel (b) indicates the average value after equilibration of the POPC–Chol50 simulation box surface area of $43.4 \pm 1.3$ nm$^2$.

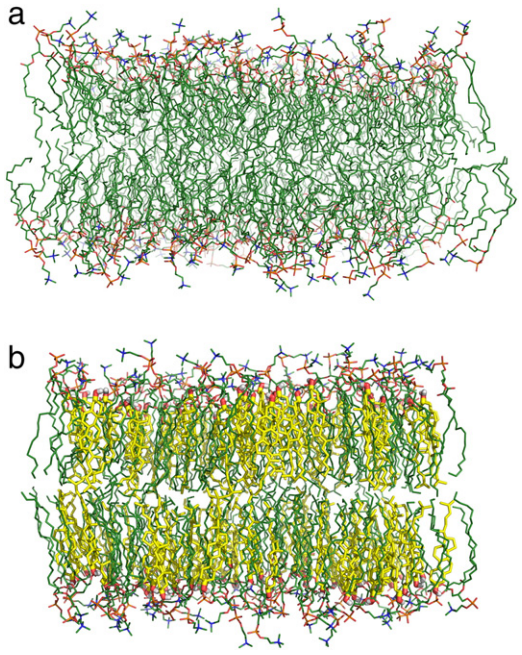


**Fig. 3.** Snapshots of the POPC (a) and POPC–Chol50 (b) bilayers at 200 ns of MD simulation. Water and hydrogen atoms are removed to better show details of the bilayers. The Chol molecules are shown as yellow sticks. The OH group of Chol is shown in standard colors as the CPK model. The remaining atoms are coded in standard colors as lines.

**Table 1**
Average membrane parameters. Average values of the surface area available to the lipid (Area); distance between average positions of phosphorus (P) atoms in the two leaflets of a bilayer (P–P distance); molecular order parameter, $S_{mol}$; tilt angle of chains, as well as the upper (δ) and lower (ω) fragments of the oleoyl-chain, for the palmitoyl- (P) and oleoyl- (O) chains of POPC; number of *trans* (# trans) and *gauche* (# gauche) rotamers per chain (torsion 11 in the O-chain is excluded); and roughness parameter, in the POPC and POPC–Chol50 bilayers. The errors are standard deviation estimates. In the case of tilt, the entries are as follows: the most probable value (for ω, "/" separates the values for both modes), and, in parentheses, the average tilt and standard deviation.

| | POPC | POPC–Chol |
|---|---|---|
| Area (Å$^2$) | $65.1 \pm 0.6$/POPC | $48.4 \pm 0.5$/POPC<br>$38.0 \pm 0.2$/Chol |
| P–P distance (Å) | $39.2 \pm 3.3$ | $45.7 \pm 2.6$ |
| $S_{mol}$ | | |
| P chain | $0.31 \pm 0.02$ | $0.61 \pm 0.02$ |
| O chain | $0.23 \pm 0.01$ | $0.50 \pm 0.02$ |
| Tilt (°) | | |
| P chain | 23 ($32.7 \pm 19.0$) | 12 ($15.6 \pm 9.2$) |
| O chain | 27 ($35.5 \pm 20.0$) | 11 ($17.1 \pm 13.6$) |
| δ | 30 ($41.6 \pm 22.3$) | 13 ($20.1 \pm 13.6$) |
| ω | 32/154 ($72.8 \pm 50.2$) | 17/161 ($50.7 \pm 54.1$) |
| # trans | | |
| P chain | $8.12 \pm 0.30$ | $9.00 \pm 0.42$ |
| O chain | $7.33 \pm 0.41$ | $7.55 \pm 0.51$ |
| # gauche | | |
| P chain | $4.22 \pm 0.30$ | $3.41 \pm 0.40$ |
| O chain | $4.81 \pm 0.09$ | $4.70 \pm 0.10$ |
| Roughness (Å) | $1.71 \pm 0.09$ | $1.32 \pm 0.07$ |

### 3.1.3. Chain order

The liquid-crystalline phase of the bilayer is characterized by a disorder of the acyl chains, the measure of which—both experimentally (*e.g.*, see Ref. [38]) and computationally (*e.g.*, see Ref. [39])—is the order parameter.

The molecular order parameter for the $n$th segment of an acyl chain, $S_{mol}$, is defined through [40]:

$$S_{mol} = \frac{1}{2}\langle 3\cos^2\theta_n - 1\rangle, \quad (1)$$

where $\theta_n$ is the instantaneous angle between the $n$th segmental vector (*i.e.*, the $(C_{n-1}, C_{n+1})$ vector linking $n-1$ and $n+1$ C atoms in the acyl chain) and the bilayer normal with corrections for sp2 hybridization of the carbon atoms linked by the double bond [39]), and $<\cdots>$ denotes both the ensemble and the time average. $S_{mol}$ profiles along the palmitoyl (P) and oleoyl (O) chain in the POPC and POPC–Chol50 bilayers are shown in Fig. 4a and b. Mean values (averaged over appropriate segmental vectors $\geq 4$) of $S_{mol}$ are given in Table 1. As can be seen from Fig. 4a and b and Table 1, Chol significantly affects the order of both the P and O chain at all depths in the membrane.

### 3.1.4. Chain tilt

In the liquid-crystalline phase (ordered or disordered) of the bilayer, there is no collective tilt of the acyl chains. Thus, assuming the axial symmetry of the system and the free rotation of chains about the normal (for each $\theta$ angle, there are $2\pi$ $\phi$ angles of equal probability), the average angle of chains with respect to the bilayer normal ($\theta$ angle) is zero. However, due to the rotation about the axis perpendicular to the bilayer normal and *trans–gauche* isomerization, the chains are tilted relative to the normal within the confines of a cone. In this analysis, we are interested only in the $\theta$ angles. Because of the comparative character of this study (no comparison with experimental values), a tilt angle $\theta$ of a PC chain was calculated from the scalar product of the vector linking the third (C23 or C33 for O and P chains, respectively, Fig. 1a) and the last carbon atom (C316 or C218 for P and O chains, respectively, Fig. 1a) in an acyl chain and the bilayer normal ($arccos\theta$). Also, tilt angles of the upper (δ, C23–C29 carbon atoms, Fig. 1a) and lower (ω, C210–C218 carbon atoms, Fig. 1a) segments of the O chain were calculated. Distributions of the tilt angles of the P and O chains, as well as those of δ and ω segments of the O chain, in the POPC and POPC–Chol50 bilayers are shown in Fig. 4c–f. The most probable (of each mode), average (calculated from the distribution), and standard deviation values are given in Table 1. Chol significantly narrows the distributions and shifts them toward lower values, decreasing both the most probable and average tilt values of both chains to ~50% of those for the POPC bilayer. The effect of Chol on the bimodal distribution of tilts for the ω segment is to separate both modes clearly, which in the POPC bilayer, partially overlap each other (Fig. 4f).

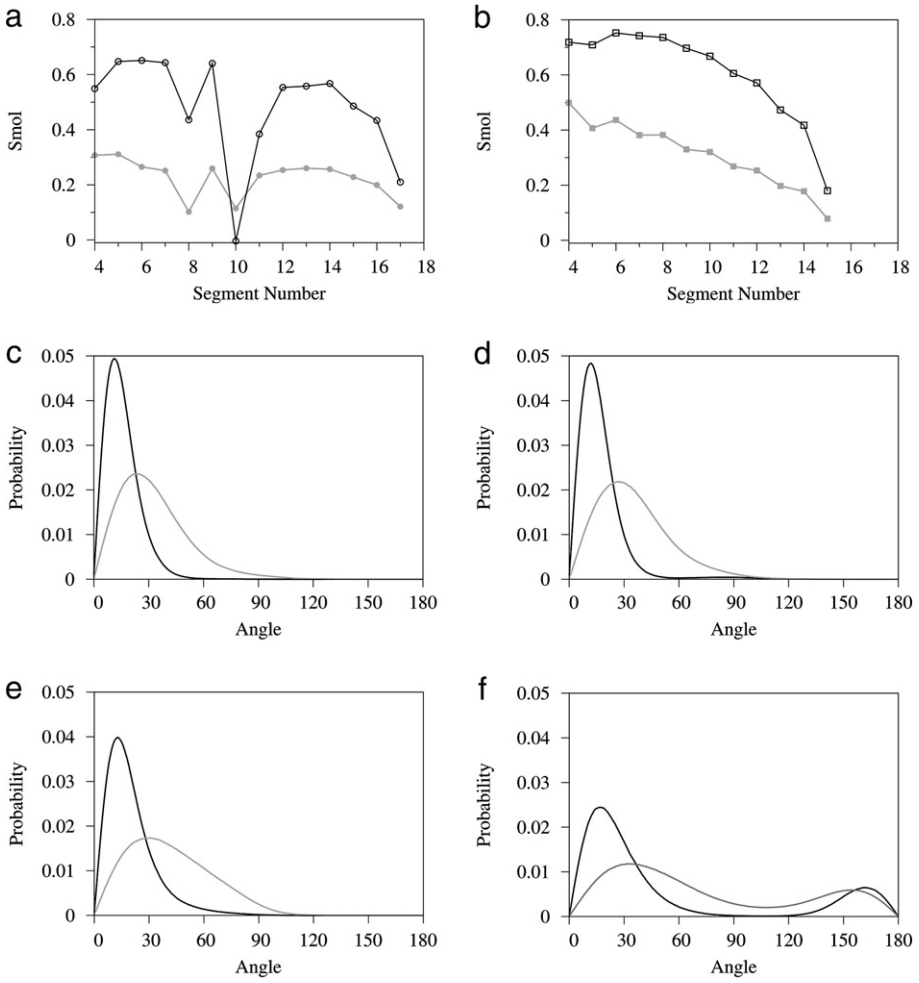


**Fig. 4.** The molecular order parameter ($S_{mol}$) profiles calculated for oleoyl (a) and palmitoyl (b) chains of POPC in the POPC (gray line) and the POPC–Chol50 (black line) bilayers. The standard deviations are of the order of 0.002. Distributions of tilt angles for palmitoyl (c) and oleoyl (d) chains as well as for the upper (e) and lower (f) segments of the oleoyl chain in the POPC (gray line) and the POPC–Chol50 (black line) bilayers.

### 3.2. Vertical alignment of atoms

Due to the liquid-crystalline character of the lipid bilayer, molecules comprising the bilayer, as well as their groups and atoms, have some motional freedom (displacements due to translational and rotational motion, as well as *trans–gauche* isomerization), and their vertical positions are distributed. In this analysis, we assess the effect of Chol on the distribution of positions along the *z*-axis of the center-of-masses (CMs) of POPC molecules and of selected atoms in the POPC and POPC–Chol50 bilayers, the latter of which to enable comparisons with spin-label experimental data [10]. When calculating distributions, changes in the *z*-coordinates of atoms, as well as the simulation box *z*-size due to scaling associated with the pressure control algorithm, were subtracted. Distributions were fitted with the Gaussian function (Fig. 5) to find their widths (Table 2 and Fig. 6). Cholesterol decreases the distribution width, Δ, for the POPC CMs in the POPC–Chol50 bilayer to ~82% of that for the POPC bilayer (Table 2). The largest effects of Chol on Δ occur for the terminal carbon atoms of the P and O chain, C316 and C218, respectively, as well as C2 (Table 2). The values in Table 2, as well as in Figs. 5 and 6, clearly indicate that Chol introduces vertical order to the bilayer, most likely by suppressing vertical fluctuations of atoms and whole molecules. Similar analysis done for the CM of Chol and selected Chol atoms in the POPC–Chol50 bilayer (Table 2 and Figs. 5 and 6) indicates that distributions are narrower than or comparably narrow to those for POPC molecules and their atoms in the

**Table 2**
Average vertical positions (*Z*) relative to the bilayer center (0) of selected POPC and Chol atoms (Fig. 1), the widths of the distributions of the positions (Δ), and relative decrease (in%) of Δ for each selected atom as well as CM of POPC and Chol molecules, in the POPC and POPC–Chol bilayers. The widths were obtained by fitting the Gaussian function to the distributions.

| Atom | POPC | | POPC–Chol | | Decrease % |
|---|---|---|---|---|---|
| | Z [nm] | Δ [m] | Z [nm] | Δ [nm] | |
| POPC | | | | | |
| N | 2.063 | 0.297 | 2.401 | 0.241 | 18.6 |
| C2 | 1.638 | 0.243 | 1.986 | 0.174 | 28.5 |
| C35 | 0.993 | 0.263 | 1.317 | 0.216 | 17.7 |
| C39 | 0.616 | 0.268 | 0.853 | 0.216 | 19.5 |
| C310 | 0.525 | 0.272 | 0.728 | 0.214 | 21.2 |
| C316 | 0.118 | 0.360 | 0.171 | 0.210 | 41.5 |
| C25 | 1.207 | 0.244 | 1.480 | 0.203 | 16.7 |
| C29 | 0.915 | 0.286 | 1.063 | 0.232 | 19.0 |
| C210 | 0.828 | 0.294 | 0.948 | 0.232 | 21.0 |
| C218 | 0.395 | 0.341[a] | 0.375 | 0.260[a] | 23.8 |
| Cholesterol | | | | | |
| O3 | – | – | 1.856 | 0.180 | |
| C17 | – | – | 0.858 | 0.179 | |
| C25 | – | – | 0.264 | 0.179 | |
| CM | | | | | |
| CM-POPC | 1.194 | 0.214 | 1.431 | 0.168 | 21.7 |
| CM-Chol | – | – | 1.060 | 0.176 | |

[a] Width of the distribution main mode (Fig. 5c).

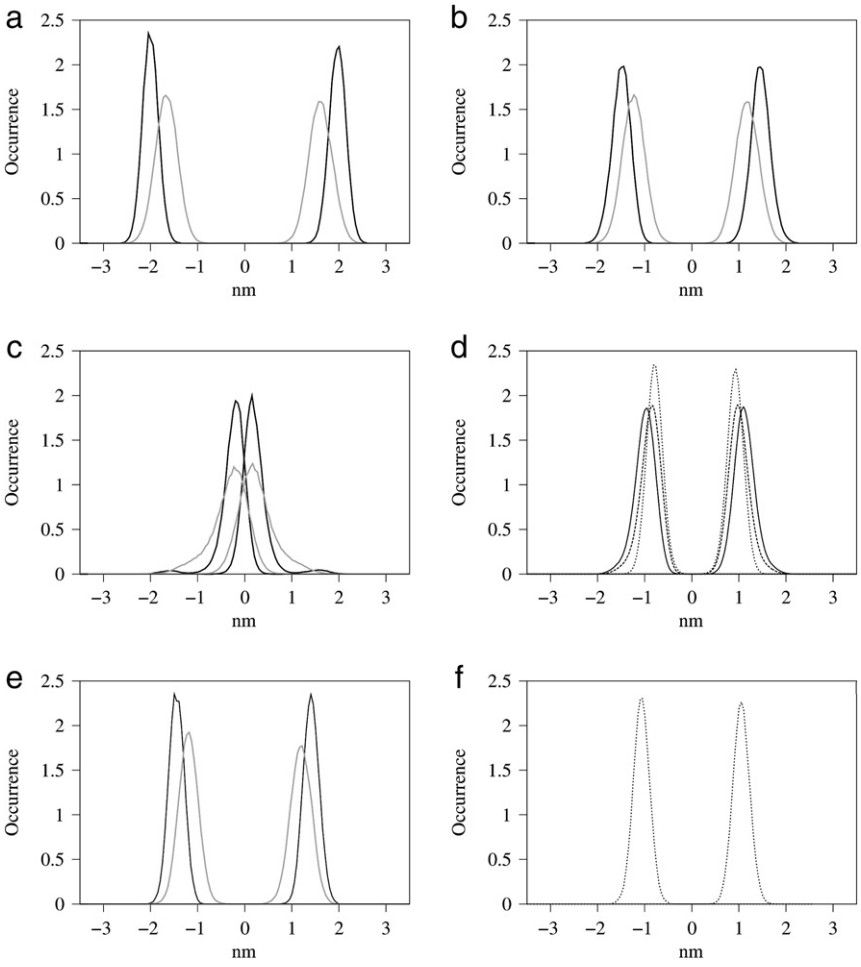


**Fig. 5.** Distributions of *z*-coordinates of atoms C2 (a); C25 (b); C218 (c); C29, C210 and C17–Chol (d); and CM of POPC (e), and CM of Chol molecules (f), in both leaflets of the POPC (gray line) and POPC–Chol50 (black line) bilayers; the dotted line corresponds to the Chol C17 atom (d), and CM Chol (f). The distributions were fitted with the Gaussian functions of widths given in Table 2. In c, the Gaussian function was fitted to the main mode.

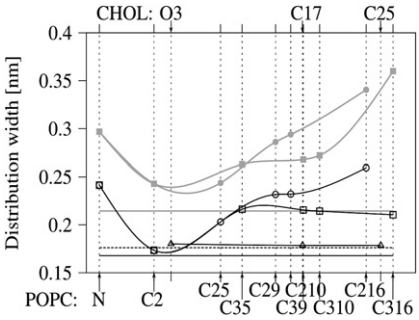


**Fig. 6.** Graphical presentations of the widths of the distributions of *z*-coordinates (Fig. 5 and Table 2) of the indicated atoms (Fig. 1) as well as CMs of POPC, and Chol molecules, in the POPC (gray line) and POPC–Chol50 (black line) bilayers. The full symbols correspond to the POPC bilayer palmitoyl (■), and oleoyl (●) chain; the open symbols correspond to the POPC–Chol50 bilayer palmitoyl (□), and oleoyl (○) chain; the symbol Δ corresponds to Chol in the POPC–Chol50 bilayer. Distribution widths of CMs of POPC (solid) and Chol (dashed) are represented by straight lines.

POPC–Chol50 bilayer. Nevertheless, the smallest values of the widths (Δ) in both the POPC and POPC–Chol50 bilayers were for atoms C2 and C25 (Fig. 1a and Table 2).

### 3.3. Smoothness of membrane surfaces

As follows, we checked if, as the result of the vertical alignment of atoms, chosen surfaces in the POPC–Chol50 bilayer are flatter than in the POPC bilayer. Analyzed surfaces were represented by contour maps computed for the last time frame of the 200-ns MD simulation (Fig. 7), for POPC C2 atoms (Fig. 1a), specifying the outer bilayer surface (Fig. 7a and b), and for terminal P chain carbon atoms, C316 (Fig. 1a), specifying the inner bilayer surface (Fig. 7c and d), of one leaflet of the POPC and POPC–Chol50 bilayers. Also, contour maps for Chol C3 (Fig. 1b) atoms in the upper and lower leaflets of the POPC–Chol50 bilayer (Fig. 7e and f) were calculated to examine if there was any correlation between the two bilayer surfaces. Fig. 7 shows that both the outer and inner surfaces of the POPC–Chol50 bilayer are significantly flatter than those in the POPC bilayer. The surfaces defined by the POPC C2 and Chol C3 atoms in the POPC–Chol50 bilayer are similar, indicating similar vertical alignment of both C2 and C3. Also, the Chol C3 surfaces in the upper and lower leaflets are comparably flat, and their shapes do not show much correlation.

The above results were obtained for one final time frame for each MD simulation. To assess the persistence of the vertical positions of the atoms, in each bilayer we selected a C2 atom that occupies the highest position on the contour maps at 200 ns, and recorded time profile of the atom's vertical position in the POPC and the POPC–Chol50 bilayer in the period between 100 and 200 ns (Fig. 8). The profiles and ranges of C2 atoms displacements (horizontal lines in Fig. 8) indicate that in the POPC–Chol50 bilayer, the *z*-coordinate of the atom fluctuates less than in the POPC bilayer. Moreover, there are significant changes in the *z*-coordinates of the atoms within 100 ns—that is, the C2 atom that occupies the highest position on the contour map at the end of the MD simulation (200 ns) changed its position several times during the course of the 100-ns MD simulation. The same applies to other C2 atoms. In effect, the surfaces of the POPC and POPC–Chol50 bilayers fluctuate. The dynamics of the C2 surfaces in both bilayers are presented as animation sequences (AS1 and AS2) in the Supplementary Material.

To explain how fluctuations in the vertical positions of C2 atoms affect bilayer smoothness and to compare numerically the smoothness of surfaces in the two bilayers, we calculated an average roughness parameter (RP) for the upper outer surface in the POPC and POPC–Chol50 bilayers along the trajectory (every 1 ps) using the formulae [41]:

$$RP = \frac{1}{n}\sum_{i=1}^{n} |z_i - \bar{z}|, \tag{2}$$

where $z_i$ is the *z*-coordinate of the *i*-th C2 atom and $\bar{z}$ is the average vertical position of all C2 atoms in the upper surface for a given time frame. Time profiles of RP are given in Fig. 9a and b. Although the values of RP fluctuate (Fig. 9a), they are consistently higher for the POPC bilayer. This is more apparent in Fig. 9b for the profiles smoothed with a 10-ns moving window. Fig. 9b also shows that RP is practically constant between 100 and 200 ns of MD simulation. The working trajectory mean values of the average RP are 1.71 ± 0.09 Å and 1.32 ± 0.07 Å for the POPC and POPC–Chol50 bilayers, respectively (Table 1). To test whether the difference between the two sets of RP values is statistically significant, the Welch two-sample *t*-test was used. It showed that the difference was statistically significant with a 95% confidence level.

Although in the POPC–Chol50 bilayer the arrangement of Chol (as well as POPC) molecules changes with time (Figs. S1 and S2, Supplementary Material), the average RP remains virtually constant. Therefore, one can conclude that the Chol smoothing effect does not depend on a particular distribution of Chol molecules in the bilayer. This result is not totally in line with previous MD simulation studies by Smondyrev and Berkowitz [42] and Zhu et al. [43] that indicated that the arrangement of Chol molecules in a PC–Chol bilayer at a fixed cholesterol mole fraction did affect certain bilayer properties. However, the authors did not analyze the smoothness of the bilayer surface.

### 3.4. Trans–gauche isomerization

*Trans–gauche* isomerization is a restricted, local rotational motion in the PC hydrocarbon chain. This motion contributes both to the $S_{mol}$ profile along the chain and to the vertical fluctuations of the chain atoms. In this analysis, average lifetime and probability of the conformation of each torsion angle along the acyl chain were calculated for POPC molecules in the POPC and POPC–Chol50 bilayers. Profiles of lifetime along the P and O chains are shown in Fig. 10. The probabilities of *trans*, *gauche*, and *skew* conformations along the PC chains for the two bilayers are shown in Fig. 11. The average numbers of *trans* and *gauche* rotamers per P and O chain in both bilayers are given in Table 1. Chol has little effect on the lifetime of the *gauche* conformation in both O and P chains. In most cases, the lifetime is slightly shorter except for torsion 13 in the O chain (Fig. 10a). However, Chol has a large effect on the lifetime of the *trans* conformation, particularly for even torsions in the P chain for which the lifetime is significantly longer (Fig. 10b), and for torsions 9 and 13, as well as torsion 4, in the O chain for which the lifetime is significantly shorter (Fig. 10a). Consequently, in the P chain, Chol increases the average number of *trans* rotamers per chain, which automatically decreases the average number of *gauche* rotamers per chain. Chol has mixed effect on probabilities of *trans* and *gauche* conformations in the O chain (Figs. 10 and 11) and in effect it has little effect on average numbers of *trans* and *gauche* rotamers per chain. The effect of Chol on the *skew* conformation lifetime and probability of torsions 10 and 12 in the O chain is slight (Figs. 10 and 11).

## 4. Discussion

Age-related cataracts are the primary cause of vision loss in the elderly population of developing countries. The early detection and prevention of cataracts require increased understanding of the physiological, biochemical, and biophysical bases of lens transparency at the cellular and molecular levels. The goal of this paper was to achieve a greater understanding of the function of Chol in the

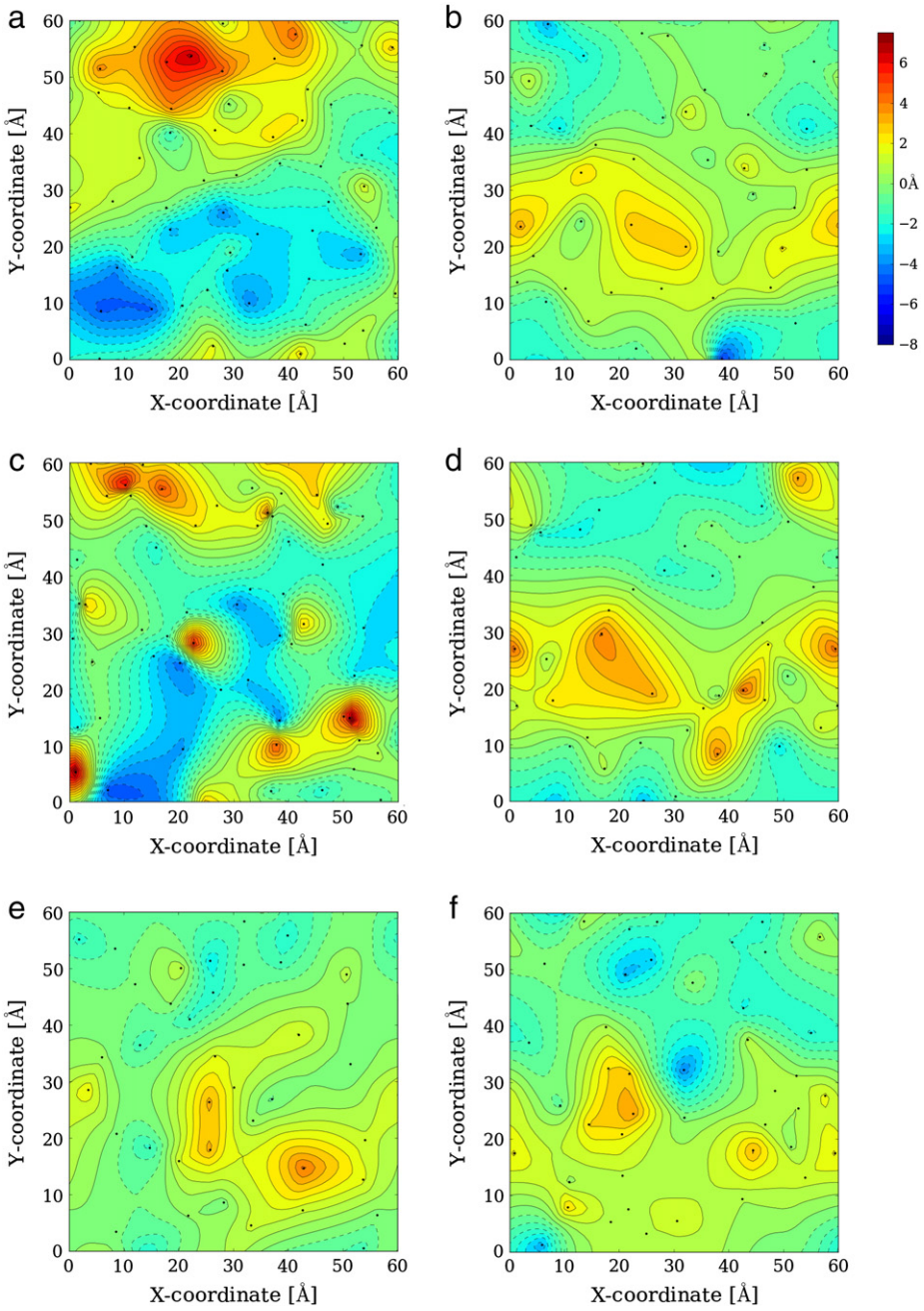


**Fig. 7.** Contour maps representing bilayer surfaces. Surfaces defined by atoms in the upper leaflet of the POPC (a and c) and POPC–Chol50 (b and d) bilayers: C2 (a and b), and the terminal carbon atoms in the palmitoyl chains, C316 (c and d). Surfaces defined by Chol C3 atoms in the upper (e) and lower (f) leaflet of the POPC–Chol50 bilayer, at the end of the respective 200-ns MD simulations.

human eye lens. In this study, we focused our attention on the properties of the phospholipid bilayer saturated with Chol, which models the phospholipid-cholesterol domain, PCD, of the fiber-cell plasma membrane of the eye lens. The molecular-level information of this bilayer cannot be obtained by calorimetric [44], diffraction [3], or magic-angle-spinning nuclear magnetic resonance [44,45] methods, which have been typically applied to investigate the lateral organization of bulk lens lipid membranes and intact lens membranes. Fortunately, EPR spin-labeling methods enabled us to obtain the missing molecular-level information on the organization and dynamics of lipid molecules in the PCD and also information, how these properties change as a function of the membrane depth [9–12]. Those studies showed that in lens lipid membranes as well as POPC bilayers that were saturated with Chol, both oxygen transport parameter and hydrophobicity profiles across the bilayer had a rectangular shape [10,11]. In liquid-ordered POPC–Chol bilayers, the rectangular shape of the oxygen transport parameter profile, with an abrupt increase close to the positions of C9 in acyl chains, is observed only for bilayers saturated with Chol (*i.e.*, containing 50 mol% Chol). This is in contrast to liquid-ordered POPC–Chol bilayers of the lowest Chol content of ~30 mol% for which the profile is bell-shaped and similar to that for bilayers without Chol. Therefore, it was concluded that saturation with Chol decreases vertical fluctuations of membrane lipids (phospholipids and cholesterol). In effect, the lipids are vertically aligned, and all Chol rings are immersed to the same membrane depth, which is close to the positions of C9 in PC acyl chains. As a result, the membrane surface is smoother compared to membranes without or with lower Chol content.

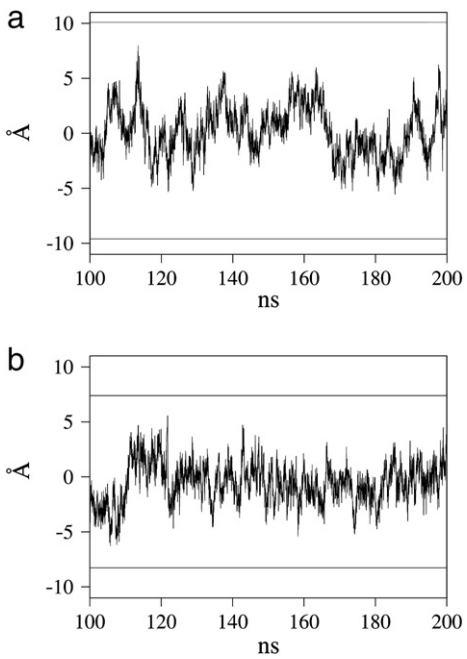


**Fig. 8.** Time profiles of the z-coordinates of C2 atom that occupied the highest positions on the contour map at 200 ns (Fig. 7a and b) for the POPC (a) and POPC–Chol50 (b) bilayers. Horizontal lines in each panel indicate the range of displacements of all C2 atoms in the upper leaflet of the bilayer during 100 ns.

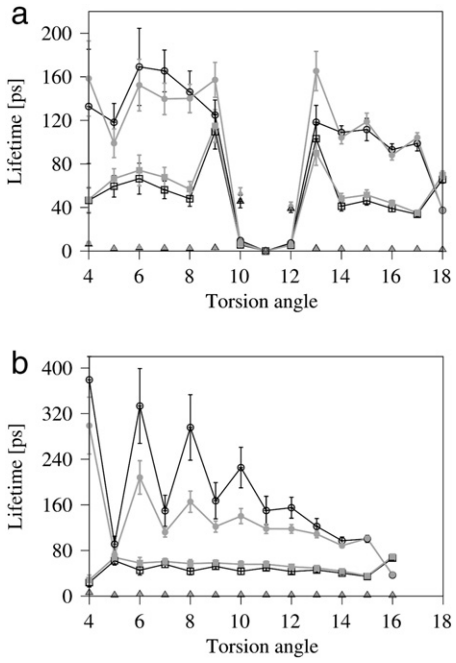


**Fig. 10.** Profiles of lifetimes of the *trans* (○,●), *gauche* (□, ■), and *skew* (Δ, ▲) conformations along oleoyl chain (a) and palmitoyl chain (b) in the POPC (●, ■, ▲, gray line) and POPC–Chol50 (○, □, Δ, black line) bilayers. The errors bars are standard deviations.

MD simulations carried out in this study confirm those conclusions. Here, we examined the vertical alignment of selected atoms in POPC and Chol molecules by calculating directly distributions of their positions along the *z*-axis in the bilayer. The width (Δ) of the distribution for each selected atom is significantly narrowed (from 17 to 42%) by the presence of a saturating amount of Chol (Table 2, Figs. 5 and 6). MD simulations also confirmed that, indeed, all Chol rings are immersed to the depth close to the positions of C9–C10 in acyl chains as the distribution for C17 (Fig. 1b) almost overlaps (Fig. 5d) with that for C210 (Fig. 1a).

The difference between ΔN (width for N atoms in the polar headgroups) and ΔC2 (Table 2) is smaller in the bilayer without Chol than in the bilayer saturated with Chol (Fig. 6). This is an important addition to our earlier experimental results, which showed that the extent of vertical fluctuations of the headgroup, measured as a displacement relative to the glycerol backbone C2 atom, increases after the addition

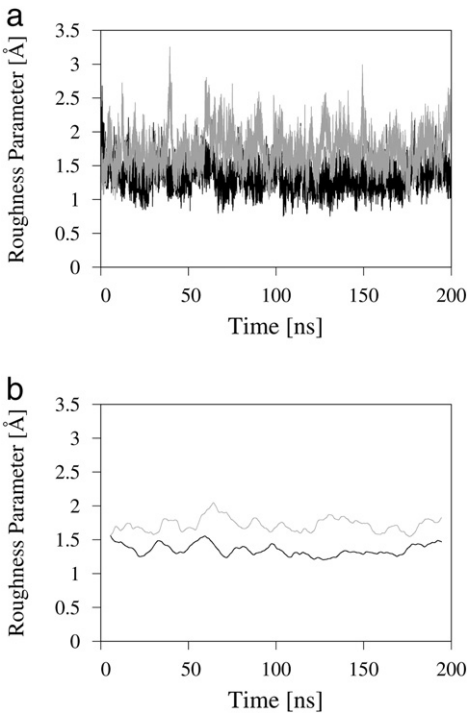


**Fig. 9.** Time profiles of the average roughness parameter (RP) calculated every 1 ps along MD trajectories for the POPC (gray line) and POPC–Chol50 (black line) bilayers. Unsmoothed profiles (a) and profiles smoothed with a 10 ns moving window (b).

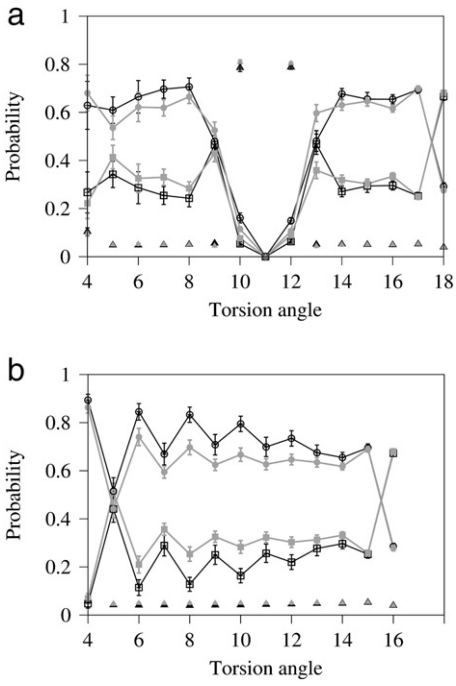


**Fig. 11.** Profiles of probabilities of *trans* (○,●), *gauche* (□, ■), and *skew* (Δ, ▲) conformations along oleoyl chain (a) and palmitoyl chain (b) in the POPC (●, ■, ▲, gray line) and POPC–Chol50 (○, □, Δ, black line) bilayers. The errors bars are standard deviations.

of a saturating amount of Chol [46], most likely because of a larger available space to the PC headgroups in the bilayer containing Chol [47], which gives them more motional freedom.

In contrast, the difference between Δs for selected atoms in the PC acyl chains and the Δ for CMs of the POPC molecules is higher in the absence, rather than the presence, of Chol (Fig.6). This indicates that the local (segmental) motion within acyl chains contributes significantly to the extent of vertical displacements, and that this motion is affected by the presence of Chol. Interestingly, this is more pronounced for the P chain than the O chain (Fig. 6). To elucidate the effect of Chol on segmental motion, analyses of the lifetimes and probabilities of *gauche* and *trans* conformations along the acyl chains were carried out. They indicated that, indeed, Chol differently affects torsion angles in the P and O chains. In the P chain, Chol significantly increases the *trans* conformation lifetime and probability, particularly for even torsion angles but practically does not affect the *gauche* conformation lifetime (Figs. 10 and 11). In effect, the average number of *trans*/P-chain increases and that of *gauche*/P-chain decreases (Table 1), thus, the P chain is more straight. Tilt-angle analysis additionally showed that the P chain in the POPC–Chol50 bilayer is also more aligned with the bilayer normal than in the POPC bilayer (Fig. 4). All these result in diminished vertical fluctuations of P chain atoms in the POPC–Chol50 bilayer.

The effect of Chol on the O chain is much less straightforward. In contrast to the P chain, Chol has a non-uniform and modest effect on the *trans* and *gauche* conformation lifetimes and probabilities in the O chain (Figs. 10 and 11). In effect, the average numbers of *trans* and *gauche* rotamers per O chain are similar both in POPC and POPC–Chol50 bilayers (Table 1).

In light of Chol's modest effect on the lifetimes and probabilities of *trans* and *gauche* rotamers in the O chain, the aligning effect of Chol on the O chain and its upper and lower fragments (δ and ω) is surprisingly high (Fig. 4d–f). In both POPC and POPC–Chol50 bilayers, there is some fraction of the ω segments in which terminal C218 atoms lie closer to the bilayer interface than C210 atoms (tilt > 90°). These fractions are responsible for the bimodal distributions of tilt angles (Fig. 4f) as well as z-coordinates of C218 (Fig. 5c). Thus, the higher values of the $S_{mol}$ profile along the O chain in the POPC–Chol50 bilayer (Fig. 4a) can be explained by the decreased average tilt of the O chains and their δ and ω segments, as well as the interplay of the probabilities of conformations of torsion angles along the chain. This higher ordering of the O chain results in a narrower distribution of the vertical positions of the chain atoms, but the effect is smaller than in the case of the P chain.

In this study, MD simulations were performed using POPC as a representative phospholipid. However, PC is the major phospholipid in animal lenses, accounting for 35 to 45% of total lipids [14], but a minor phospholipid in human lenses, accounting for only ~11% of total lipids [14]. EPR experiments were performed on pig- and cow-lens lipid membranes and, therefore, on lipid bilayers made of POPC, which was the main reason for its usage. Additionally, computer models of POPC membranes are well established and investigated. Recent EPR measurements with sphingomyelin bilayers (the major phospholipid of human lenses [14]) have confirmed that a saturating amount of Chol also decreases vertical fluctuations in these bilayers [20].

The initial regular distribution of POPC and Chol in the bilayer (Fig. S1a, Supplementary Material) was significantly disturbed after only 100 ns of MD simulation, showing fluctuations of the local Chol concentration (Fig. S1b, Supplementary Material). However, the average RP (Eq. (2)) changes little with time, particularly after bilayer equilibration (Fig. 9b). Therefore, we concluded that local Chol fluctuations do not affect bulk smoothness of the membrane surface. This is supported by the fact that in phosphatidylcholine [21], sphingomyelin [20], and lens lipid [9,10,12] membranes saturated with Chol, cholesterol-rich domains do not form and membranes are homogenous on a time scale of 100 ns or longer. Thus, membrane smoothness is not an artifact of the selected distribution of Chol but the property induced by the saturating Chol content.

One of the principal properties of the lens is transparency. Transparency of the eye lens is reduced by light-scattering from different lens elements. Intensive studies have been carried out on this subject and indicate that significant light-scattering may arise from protein density fluctuations [48] and multilamellar bodies [49]. The contribution of lens membrane lipids to light-scattering was extensively discussed by Tang et al. [50,51], Michael et al. [52], and Bettelheim and Paunovic [53]. However, light-scattering by the human lens is a very complex physical phenomenon, and contributions from different lens elements are difficult to separate as light-scattering depends on their mutual interaction [50,54,55]. In the case of membranes, light-scattering has its origins in the structural irregularities at the surface and in the bulk of the membrane. Bulk scattering might be described by Rayleigh scattering, as the scattering objects (molecules, density fluctuations) are smaller than the incident light wavelength. Surface scattering arises from random roughness of the membrane surface [56], described by the average roughness parameter (Eq. (2)). Contribution to surface light-scattering arising from surface irregularities of heights less than 2 nm was measured experimentally in Ref. [57]. The level of light-scattering at each lipid membrane surface is certainly low. However, in the human lens, the number of cell layers is 1000 to 2000. Therefore, light crosses thousands of cell membranes, and scattering is amplified at each surface [56]. Thus, cholesterol-induced smoothing of the bilayer surface might indeed reduce light-scattering by the lens. Accordingly, based on the present MD simulation results and previous data from EPR spin-labeling measurements, we hypothesize that cholesterol-induced smoothing of the membrane surface should decrease light-scattering and help to maintain lens transparency. This hypothesis will be tested in our future work.

In this article, we have concentrated on the vertical fluctuations of lipid molecules and their atoms in the bilayer. Larger-scale vertical fluctuations of lipid bilayers are thoroughly analyzed in Ref. [58] but discussion of their contribution to light-scattering by fiber-cell membranes is beyond the scope of this study.

In conclusion, the results of the MD simulations presented here, together with the results of our EPR measurements cited above, have broadened our knowledge and allowed us to better characterize cholesterol-dependent, liquid-ordered membranes saturated with Chol, which have not been investigated extensively thus far and are a major addition to the known condensing effect of Chol [27,37,59,60]. Our results have also contributed to a better understanding of the function of Chol in the fiber-cell membranes of the human eye lens, especially in consideration of suggestions in the literature that a high amount of Chol in the membrane, together with Chol bilayer domains, helps to maintain lens transparency [3,6,7].

Supplementary materials related to this article can be found online at doi:10.1016/j.bbamem.2011.10.023.

## Acknowledgements

This work was supported by grants TW008052 and EY015526 of the National Institutes of Health. Some calculations were performed on the cluster purchased under contract No. POIG.02.01.00-12-167/08, project MCB.

## References

[1] L.K. Li, L. So, A. Spector, Age-dependent changes in the distribution and concentration of human lens cholesterol and phospholipids, Biochim. Biophys. Acta 917 (1987) 112–120.
[2] R.J. Truscott, Age-related nuclear cataract: a lens transport problem, Ophthalmic Res. 32 (2000) 185–194.
[3] R.P. Mason, T.N. Tulenko, R.F. Jacob, Direct evidence for cholesterol crystalline domains in biological membranes: role in human pathobiology, Biochim. Biophys. Acta 1610 (2003) 198–207.

[4] V. Pata, N. Dan, Effect of membrane characteristics on phase separation and domain formation in cholesterol–lipid mixtures, Biophys. J. 88 (2005) 916–924.
[5] M. Raguz, L. Mainali, J. Widomska, W.K. Subczynski, The immiscible cholesterol bilayer domain exists as an integral part of phospholipid bilayer membranes, Biochim. Biophys. Acta 1808 (2011) 1072–1080.
[6] D. Borchman, R.J. Cenedella, O.P. Lamba, Role of cholesterol in the structural order of lens membrane lipids, Exp. Eye Res. 62 (1996) 191–197.
[7] R.F. Jacob, R.J. Cenedella, R.P. Mason, Evidence for distinct cholesterol domains in fiber cell membranes from cataractous human lenses, J. Biol. Chem. 276 (2001) 13573–13578.
[8] R.F. Jacob, R.J. Cenedella, R.P. Mason, Direct evidence for immiscible cholesterol domains in human ocular lens fiber cell plasma membranes, J. Biol. Chem. 274 (1999) 31613–31618.
[9] M. Raguz, J. Widomska, J. Dillon, E.R. Gaillard, W.K. Subczynski, Characterization of lipid domains in reconstituted porcine lens membranes using EPR spin-labeling approaches, Biochim. Biophys. Acta 1778 (2008) 1079–1090.
[10] J. Widomska, M. Raguz, J. Dillon, E.R. Gaillard, W.K. Subczynski, Physical properties of the lipid bilayer membrane made of calf lens lipids: EPR spin labeling studies, Biochim. Biophys. Acta 1768 (2007) 1454–1465.
[11] J. Widomska, M. Raguz, W.K. Subczynski, Oxygen permeability of the lipid bilayer membrane made of calf lens lipids, Biochim. Biophys. Acta 1768 (2007) 2635–2645.
[12] M. Raguz, J. Widomska, J. Dillon, E.R. Gaillard, W.K. Subczynski, Physical properties of the lipid bilayer membrane made of cortical and nuclear bovine lens lipids: EPR spin-labeling studies, Biochim. Biophys. Acta 1788 (2009) 2380–2388.
[13] R.M. Broekhuyse, Lipids in tissue of the eye. IV. Influence of age and species differences on the phospholipid composition of the lens, Biochim. Biophys. Acta 218 (1970) 546–548.
[14] J.M. Deeley, T.W. Mitchell, X. Wei, J. Korth, J.R. Nealon, S.J. Blanksby, R.J. Truscott, Human lens lipids differ markedly from those of commonly used experimental animals, Biochim. Biophys. Acta 1781 (2008) 288–298.
[15] D. Borchman, M.C. Yappert, M. Afzal, Lens lipids and maximum lifespan, Exp. Eye Res. 79 (2004) 761–768.
[16] M. Rujoi, R. Estrada, M.C. Yappert, In situ MALDI-TOF MS regional analysis of neutral phospholipids in lens tissue, Anal. Chem. 76 (2004) 1657–1663.
[17] R. Estrada, A. Puppato, D. Borchman, M.C. Yappert, Reevaluation of the phospholipid composition in membranes of adult human lenses by (31)P NMR and MALDI MS, Biochim. Biophys. Acta 1798 (2010) 303–311.
[18] A. Kusumi, W.K. Subczynski, J.S. Hyde, Oxygen transport parameter in membranes as deduced by saturation recovery measurements of spin–lattice relaxation times of spin labels, Proc. Natl. Acad. Sci. U.S.A. 79 (1982) 1854–1858.
[19] W.K. Subczynski, J.S. Hyde, A. Kusumi, Effect of alkyl chain unsaturation and cholesterol intercalation on oxygen transport in membranes: a pulse ESR spin labeling study, Biochemistry 30 (1991) 8578–8590.
[20] L. Mainali, M. Raguz, W.K. Subczynski, Phase-separation and domain formation in cholesterol–sphingomyelin mixture: pulse EPR oxygen probing, Biophys. J. 101 (2011) 837–846.
[21] W.K. Subczynski, A. Wisniewska, J.S. Hyde, A. Kusumi, Three-dimensional dynamic structure of the liquid-ordered domain in lipid membranes as examined by pulse-EPR oxygen probing, Biophys. J. 92 (2007) 1573–1584.
[22] W.K. Subczynski, M. Raguz, J. Widomska, Studying lipid organization in biological membranes using liposomes and EPR spin labeling, in: V. Weissig (Ed.), Methods in Molecular Biology, "Liposomes, Methods and Protocols", The Humana Press, Totowa, NJ, 2010, pp. 247–269.
[23] W.K. Subczynski, J. Widomska, J.B. Feix, Physical properties of lipid bilayers from EPR spin labeling and their influence on chemical reactions in a membrane environment, Free Radic. Biol. Med. 46 (2009) 707–718.
[24] T. Rog, M. Pasenkiewicz-Gierula, I. Vattulainen, M. Karttunen, Ordering effects of cholesterol and its analogues, Biochim. Biophys. Acta 1788 (2009) 97–121.
[25] B. Hess, C. Kutzner, D. van der Spoel, E. Lindahl, GROMACS 4: algorithms for highly efficient, load-balanced, and scalable molecular simulation, J. Chem. Theory Comput. 4 (2008) 435–447.
[26] H.-S. Shieh, L.G. Hoard, C.E. Nordman, The structure of cholesterol, Acta Crystallogr. B37 (1981) 1538–1543.
[27] T. Rog, M. Pasenkiewicz-Gierula, Cholesterol effects on a mixed-chain phosphatidylcholine bilayer: a molecular dynamics simulation study, Biochimie 88 (2006) 449–460.
[28] W.L. Jorgensen, D.S. Maxwell, J. Tirado-Rives, Development and testing of the OPLS all-atom force field on conformational energetics and properties of organic liquids, J. Am. Chem. Soc. 118 (1996) 11225–11236.
[29] W.L. Jorgensen, J. Chandrasekhar, J.D. Madura, R.W. Impey, M.L. Klein, Comparison of simple potential functions for simulating liquid water, J. Chem. Phys. 79 (1983) 926–935.
[30] B. Hess, H. Bekker, H.J.C. Berendsen, J.G.E.M. Fraaije, LINCS: a linear constraint solver for molecular simulations, J. Comput. Chem. 18 (1997) 1463–1472.
[31] U. Essmann, L. Perera, M.L. Berkowitz, T. Darden, H. Lee, L.G. Pedersen, A smooth particle mesh Ewald method, J. Chem. Phys. 103 (1995) 8577–8593.
[32] J. Seelig, N. Waespe-Šarčević, Molecular order in cis and trans unsaturated phospholipid bilayers, Biochemistry 17 (1978) 3310–3315.
[33] W.G. Hoover, Canonical dynamics: equilibrium phase-space distributions, Phys. Rev. A 31 (1985) 1695–1697.
[34] M. Parrinello, A. Rahman, Polymorphic transitions in single crystals: a new molecular dynamics method, J. Appl. Phys. 52 (1981) 7182–7190.
[35] M. Pasenkiewicz-Gierula, T. Rog, K. Kitamura, A. Kusumi, Cholesterol effects on the phosphatidylcholine bilayer polar region: a molecular simulation study, Biophys. J. 78 (2000) 1376–1389.
[36] T. Rog, M. Pasenkiewicz-Gierula, Cholesterol effects on the phosphatidylcholine bilayer nonpolar region: a molecular simulation study, Biophys. J. 81 (2001) 2190–2202.
[37] P.A. Hyslop, B. Morel, R.D. Sauerheber, Organization and interaction of cholesterol and phosphatidylcholine in model bilayer membranes, Biochemistry 29 (1990) 1025–1038.
[38] J. Seelig, A. Seelig, Lipid conformation in model membranes and biological membranes, Q. Rev. Biophys. 13 (1980) 19–61.
[39] H. Heller, M. Schaefer, K. Schulten, Molecular dynamics simulation of a bilayer of 200 lipids in the gel and liquid-crystal phases, J. Phys. Chem. 97 (1993) 8343–8360.
[40] W.L. Hubbell, H.M.J. McConnell, Molecular motion in spin-labelled phospholipids and biomembranes, J. Am. Chem. Soc. 93 (1971) 314–326.
[41] E.S. Gadelmawla, M.M. Koura, T.M.A. Maksoud, I.M. Elewa, H.H. Soliman, Roughness parameters, J. Mater. Process. Technol. 123 (2002) 133–145.
[42] A.M. Smondyrev, M.L. Berkowitz, Structure of dipalmitoylphosphatidylcholine/cholesterol bilayer at low and high cholesterol concentrations: molecular dynamics simulation, Biophys. J. 77 (1999) 2075–2089.
[43] Q. Zhu, K.H. Cheng, M.W. Vaughn, Molecular dynamics studies of the molecular structure and interactions of cholesterol superlattices and random domains in an unsaturated phosphatidylcholine bilayer membrane, J. Phys. Chem. B 111 (2007) 11021–11031.
[44] R.M. Epand, Cholesterol in bilayers of sphingomyelin or dihydrosphingomyelin at concentrations found in ocular lens membranes, Biophys. J. 84 (2003) 3102–3110.
[45] W. Guo, J.A. Hamilton, 13C MAS NMR studies of crystalline cholesterol and lipid mixtures modeling atherosclerotic plaques, Biophys. J. 71 (1996) 2857–2868.
[46] W.K. Subczynski, A. Wisniewska, J.-J. Yin, J.S. Hyde, A. Kusumi, Hydrophobic barriers of lipid bilayer membranes formed by reduction of water penetration by alkyl chain unsaturation and cholesterol, Biochemistry 33 (1994) 7670–7681.
[47] K. Murzyn, T. Rog, G. Jezierski, Y. Takaoka, M. Pasenkiewicz-Gierula, Effects of phospholipid unsaturation on the membrane/water interface: a molecular simulation study, Biophys. J. 81 (2001) 170–183.
[48] G.B. Benedek, Cataract as a protein condensation disease: the Proctor Lecture, Invest. Ophthalmol. Vis. Sci. 38 (1997) 1911–1921.
[49] K.O. Gilliland, C.D. Freel, C.W. Lane, W.C. Fowler, M.J. Costello, Multilamellar bodies as potential scattering particles in human age-related nuclear cataracts, Mol. Vis. 7 (2001) 120–130.
[50] D. Tang, D. Borchman, A.K. Schwarz, M.C. Yappert, G.F.J.M. Vrensen, J. van Marle, D.B. DuPré, Light scattering of human vasicles in vitro, Exp. Eye Res. 76 (2003) 605–612.
[51] D. Tang, D. Borchman, M.C. Yappert, G.F. Vrensen, V. Rasi, Influence of age, diabetes, and cataract on calcium, lipid–calcium, and protein–calcium relationships in human lenses, Invest. Ophthalmol. Vis. Sci. 44 (2003) 2059–2066.
[52] R. Michael, J. van Marle, G.F. Vrensen, T.J. van den Berg, Changes in the refractive index of lens fibre membranes during maturation–impact on lens transparency, Exp. Eye Res. 77 (2003) 93–99.
[53] F.A. Bettelheim, M. Paunovic, Light scattering of normal human lens. Application of random density and orientation function theory, Biophys. J. 26 (1997) 85–100.
[54] D. Borchman, D. Tang, Binding capacity of alpha-crystallin to bovine lens lipids, Exp. Eye Res. 63 (1996) 407–410.
[55] D. Tang, D. Borchman, M.C. Yappert, R.J. Cenedella, Influence of cholesterol on the interaction of alpha-crystallin with phospholipids, Exp. Eye Res. 66 (1998) 559–567.
[56] C. Amra, C. Grezes-Besset, L. Bruel, Comparison of surface and bulk scattering in optical multilayers, Appl. Opt. 32 (1993) 5492–5503.
[57] C. Amra, Light scattering from multilayer optics. I. Tools of investigation, Opt. Soc. Am. A 11 (1994) 197–210.
[58] E.G. Brandt, A.R. Braun, J.N. Sachs, J.F. Nagle, O. Edholm, Interpretation of fluctuation spectra in lipid bilayer simulations, Biophys. J. 100 (2011) 2104–2111.
[59] J.M. Smaby, H.L. Brockman, R.E. Brown, Cholesterol's interfacial interactions with sphingomyelins and phosphatidylcholines: hydrocarbon chain structure determines the magnitude of condensation, Biochemistry 33 (1994) 9135–9142.
[60] T. Rog, M. Pasenkiewicz-Gierula, Cholesterol effects on the phospholipid condensation and packing in the bilayer: a molecular simulation study, FEBS Lett. 502 (2001) 68–71.
[61] M. Sundaralingam, Molecular structures and conformations of the phospholipids and sphingomyelins, Ann. N. Y. Acad. Sci. 195 (1972) 324–355.